Journal of General Virology (2013), **94**, 1818–1826 DOI 10.1099/vir.0.052951-0

Rotavirus core shell subdomains involved in polymerase encapsidation into virus-like particles

Crystal E. Boudreaux,[1]† Donald C. Vile,[1,2]† Brian L. Gilmore,[1] Justin R. Tanner,[1] Deborah F. Kelly[1,2,3] and Sarah M. McDonald[1,2,4]

Correspondence
Sarah M. McDonald
mcdonaldsa@vtc.vt.edu

[1]Virginia Tech Carilion Research Institute, Roanoke, VA, USA

[2]Virginia Tech Carilion School of Medicine, Roanoke, VA, USA

[3]Department of Biological Sciences, Virginia Tech, Blacksburg, VA, USA

[4]Department of Biomedical Sciences and Pathobiology, Virginia-Maryland Regional College of Veterinary Medicine, Blacksburg, VA, USA

The triple-layered rotavirus virion encases an 11-segmented, dsRNA genome and 11–12 copies of the viral polymerase (VP1). VP1 transcribes and replicates the genome while tethered beneath the VP2 core shell. Genome replication (i.e. minus-strand RNA synthesis) by VP1 occurs in association with core assembly. During this process, VP2 directly engages VP1, thereby (i) packaging the polymerase into a nascent core and (ii) triggering the enzyme to initiate minus-strand RNA synthesis on bound plus-strand RNA templates. Recent work has shed light on VP2 regions important for VP1 enzymic activity. In the current study, we sought to investigate VP2 subdomains involved in the encapsidation of VP1 into recombinant virus-like particles (VLPs), which are formed of VP2 and the middle layer virion protein (VP6). We showed that strain SA11 VLPs efficiently encapsidated SA11 VP1, but not the genetically divergent Bristol VP1. VLPs made with an SA11 VP2 mutant lacking residues 1–10 of the amino-terminal domain (NTD) were still able to encapsidate VP1; however, removal of the entire NTD (residues 1–102) completely abolished polymerase packaging. We also showed that a chimeric VP2 protein containing the NTD and dimer-forming subdomain of strain Bristol VP2 can efficiently encapsidate SA11 VP1. These results suggest that the VP2 NTD and dimer-forming subdomain play important, albeit non-specific, roles in both VP1 packaging and activation. When combined with previous work, the results of this study support the notion that the same VP2 regions that engage VP1 during activation are also involved in packaging the enzyme into the core.

Received 5 March 2013
Accepted 15 April 2013

INTRODUCTION

Rotaviruses are important paediatric gastrointestinal pathogens that exist as non-enveloped, triple-layered particles (Estes & Kapikian, 2007; Parashar *et al.*, 2009). The outer $T=13$ layer of the rotavirus virion is comprised of the VP7 glycoprotein and is embedded with numerous copies of the VP4 spike attachment protein (Fig. 1a). The $T=13$ middle virion layer is made up entirely of VP6, and the innermost $T=1$ core shell is formed solely of VP2 (Pesavento *et al.*, 2006). Packaged within the particle interior are 11 dsRNA genome segments and 11–12 copies each of the viral RNA-dependent RNA polymerase (VP1) and RNA capping enzyme (VP3) (Prasad *et al.*, 1996). VP1 and VP3 mediate RNA synthesis while anchored beneath the VP2 shell, near the fivefold icosahedral vertices (Estrozi *et al.*, 2013; Prasad *et al.*, 1996). During viral transcription, VP1 polymerases within VP2-VP6 double-layered particles (DLPs) synthesize plus-strand RNAs (+RNAs) using the minus-strands of dsRNA genome segments as templates (Jayaram *et al.*, 2004). These +RNAs acquire a 5′ cap by VP3 prior to their egress from aqueous fivefold channels that traverse the VP2-VP6 layers of DLPs (Lawton *et al.*, 1997a). In contrast to transcription, which occurs within an intact subviral particle, genome replication is thought to occur in association with a partially assembled VP2 core shell (Guglielmi *et al.*, 2010; Patton & Spencer, 2000). More specifically, VP1 polymerases that are presumably tethered to decameric units of VP2 perform minus-strand synthesis on assorted +RNAs to create the 11 dsRNA segments. In the process of genome replication, the core shell is suggested to close, forming an intact sphere that encapsidates VP1, VP3 and dsRNA (McDonald & Patton, 2011a). Thus, interaction(s) between VP1 and VP2 at this stage of the viral life cycle are critical for (i) packaging the polymerases into the nascent virion and for (ii) triggering the enzymes to initiate minus-strand RNA synthesis.

†These authors contributed equally to this paper.

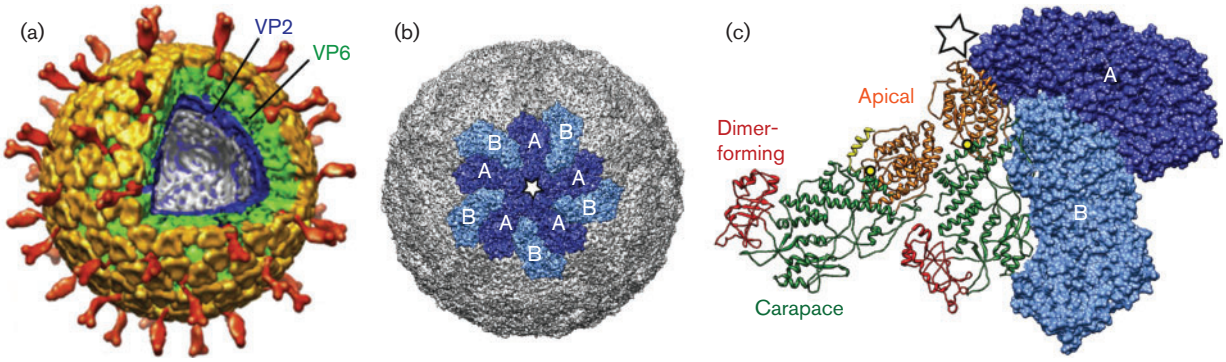

Fig. 1. Structure of the rotavirus virion and VP2 core shell. (a) Cut-away view of the complete rotavirus virion based on cryo-EM image reconstructions. This image was adapted from McClain *et al.* (2010). The two outer capsid proteins are shown in yellow (VP7) and red (VP4). The middle layer protein (VP6) is shown in green; the innermost $T=1$ VP2 core shell is shown in dark blue. (b) The VP2 core shell of a DLP crystal (PDB#3KZ4) is shown alone, with each of the 120 VP2 monomers depicted in surface representation. Five A-VP2 and five B-VP2 monomers of a central decamer are coloured dark blue and light blue, respectively. The location of the fivefold axis is depicted with a star. (c) Inside view of two neighbouring VP2 A-B dimers. One of the dimers is depicted in surface representation and coloured dark blue and light blue, respectively. The other dimer is depicted in ribbon representation and coloured according to subdomains: apical (orange), carapace (green) and dimer-forming (red). The resolved portion of the VP2 NTD in the B-VP2 monomer of this structure (residues ~81–100) is coloured yellow. The location of the fivefold axis is shown with a star as in (b), and the positions of amino-terminal residue 101 is indicated on each monomer with a yellow dot.

High-resolution structures of the VP2 core shell in the context of a DLP or mature rotavirus virion have been determined by using cryo-electron microscopy (cryo-EM) or X-ray crystallography (Li *et al.*, 2009; McClain *et al.*, 2010; Settembre *et al.*, 2011; Zhang *et al.*, 2008). In these structures, the VP2 core shell is organized into 12 decameric units (Fig. 1b). Each VP2 decamer comprises two chemically identical VP2 conformers (A-VP2 and B-VP2). Five A-VP2 conformers encircle the icosahedral fivefold axes, while five B-VP2 conformers sit further back from the fivefold axis in-between A-VP2 units (Fig. 1b). A monomer of VP2 is defined into two separate domains: (i) the amino-terminal domain (NTD), made up of residues ~1–100 and (ii) the principal scaffold domain, made up of residues ~101–880. The VP2 NTD cannot be fully resolved in the known structures, most probably because it forms a flexible protein region. However, the NTDs of neighbouring monomers have been suggested to multimerize beneath the icosahedral fivefold axes (McClain *et al.*, 2010). The VP2 principal scaffold domain is structurally distinct from the inwardly protruding NTD and makes up the actual core shell layer. This domain folds into a thin, comma-shaped plate and is subdivided into apical, carapace and dimer-forming subdomains (Fig. 1c). Hinge regions between the apical and carapace subdomains afford VP2 the flexibility to adopt A-VP2 and B-VP2 conformations (McClain *et al.*, 2010). Recent analysis of the DLP X-ray crystallographic data of the group A bovine rotavirus strain UK indicates that VP1 is localized to the inner face of the VP2 principal scaffold domain, just off-centre from the fivefold axis, with a binding footprint that overlaps the apical subdomains of neighbouring A-B VP2 conformers in a decamer (Estrozi *et al.*, 2012). Portions of the VP2 NTD are also detected near VP1, perhaps forming tethers that support the polymerase. Thus, in the context of a static DLP structure, both the NTD and the apical subdomains of the VP2 core shell directly bind VP1. Nonetheless, the functional significance of these VP1–VP2 interactions during polymerase packaging and activation is not fully understood.

Previous studies have employed recombinant proteins and an *in vitro* minus-strand RNA synthesis assay to shed light on VP2 regions critical for VP1 activation (McDonald & Patton, 2011b; Patton *et al.*, 1997). Using this approach, it was shown that deletion of the first 10 residues from the group A simian rotavirus strain SA11 VP2 NTD severely diminishes the capacity of the core shell protein to activate strain SA11 VP1 (McDonald & Patton, 2011b). It was also demonstrated that residues of the VP2 principal scaffold domain are critical for polymerase interactions. Using chimeric VP2 proteins, it was shown that strain-specific *in vitro* SA11 VP1 activation correlates with the apical and/or carapace subdomains, rather than with the NTD (McDonald & Patton, 2011b). The multimeric status of VP2 is also thought be important for VP1 interaction leading to enzymic activation. The ratio of VP1:VP2 for maximal *in vitro* minus-strand RNA synthesis is 1 : 10, suggestive of a monomer–decamer interaction (Patton *et al.*, 1997; Tortorici *et al.*, 2003). It is important to note, however, that the *in vitro* minus-strand RNA synthesis assay does not recapitulate core assembly; neither VP1 nor the replicated nascent dsRNA are encapsidated within a particle.

To study protein–protein interactions involved in rotavirus core assembly and polymerase packaging, an approach was developed that relies on the capacity of VP2 to form soluble, stable, recombinant virus-like particles (VLPs) when co-expressed from a baculovirus vector along with VP6 in *Spodoptera frugiperda* (Sf9) cells (Crawford *et al.*, 1994; Zeng *et al.*, 1996). The double-layered VLPs lack genomic dsRNA, but are still able to incorporate VP1 (and/or VP3) when they are also expressed in the insect cells (Zeng *et al.*, 1996). Using this method, it was shown that deletion of residues 1–92 from the group A bovine rotavirus strain RF VP2 NTD does not inhibit VLP formation, but such mutant particles do not efficiently encapsidate SA11 VP1 (Zeng *et al.*, 1998). In the current study, we tested the encapsidation efficiency of SA11 VP1 into cognate SA11 VLPs and compared that to the encapsidation efficiency of a genetically divergent, non-cognate VP1 derived from the group C rotavirus strain Bristol (i.e. Bristol VP1). We also used truncation and chimeric mutant VP2 proteins to analyse the importance of various core shell regions for SA11 VP1 encapsidation. Our results show that, in general, VP2 subdomains important for VP1 packaging overlap with those known to be important for VP1 activation, suggesting that these events are tightly coupled during core assembly.

RESULTS AND DISCUSSION

Efficient encapsidation of SA11 VP1, but not Bristol VP1, into SA11 VLPs

We first examined the efficiency of VP1 encapsidation into recombinant VLPs. Sf9 cells were infected with baculoviruses expressing SA11 VP2 and SA11 VP6. The cells were then also co-infected with baculoviruses expressing VP1 of either the cognate strain SA11 or the divergent strain Bristol. SA11 VP1 and Bristol VP1 are structurally conserved, but share $<46\,\%$ amino acid sequence identity (McDonald *et al.*, 2009). As a control, cells were infected with baculoviruses expressing only the capsid proteins, but not VP1. To verify recombinant protein expression, a sample of each of the infected Sf9 cells was taken at 3 days post-infection (p.i.), and the lysates were analysed by SDS-PAGE and silver staining (Fig. 2a). The results show that proteins corresponding to the molecular masses of SA11 VP2 (102 kDa) and SA11 VP6 (45 kDa) were detected in all three Sf9 cell lysates, suggesting that the capsid proteins were readily expressed (Fig. 2a). A 125 kDa protein with a similar electrophoretic migration rate as pure, recombinant SA11 VP1 (rVP1) was detected in lysates derived from cells co-infected with the VP1-expressing baculoviruses (Fig. 2a). This result suggests that SA11 VP1 and Bristol VP1 were expressed in co-infected cells and were available for packaging into VLPs.

Having verified protein expression, the cell culture supernatants from the infected Sf9 cells were harvested at 5 days p.i., and protein complexes were purified from the medium using differential centrifugation and caesium chloride (CsCl) gradient fractionation. Negative-stain EM was used to analyse the morphology of the proteins in collected gradient fractions (Fig. 2b). We found that proteins banding in CsCl at ~1.28–1.30 g cm^{-3} contained VLPs with an ultrastructure that closely resembled that of native DLPs (Fig. 2b). VLPs were consistently darker in their centres, probably because they lack genome, and collapse during negative staining (Fig. 2b). VLPs generated by co-expression of SA11 VP2 and SA11 VP6 (S2/S6 VLPs) in the presence of either SA11 VP1 (S1/S2/S6 VLPs) or Bristol VP1 (B1/S2/S6 VLPs) were morphologically indistinguishable at this resolution (Fig. 2b).

To determine whether VP1 was encapsidated into the S1/S2/S6 or B1/S2/S6 VLPs, the purified preparations were analysed by SDS-PAGE and silver staining (Fig. 3a). While the SA11 VP2 and SA11 VP6 capsid proteins were equivalently detected in all three samples, only the S1/S2/S6 VLPs showed a strongly stained 125 kDa VP1 band (Fig. 3a). A very faint VP1 band was occasionally detected in the B1/S2/S6 VLPs (Fig. 3a). Quantification of the VP1 and VP2 protein levels of VLPs from four independent experiments revealed that only the stoichiometry of the S1/S2/S6 preparations was consistent with that of native DLPs (Fig. 3b). Specifically, the percentage of VP1 relative to VP2 in S1/S2/S6 VLPs approximated 10.0 ($9.0 \pm 1.3\,\%$), while that in the B1/S2/S6 VLPs was reduced ($1.0 \pm 1.5\,\%$) (Fig. 3b). This result suggests that SA11 VP1 was efficiently engaged by SA11 VP2 and incorporated into VLPs with a 1 : 10 stoichiometry. In contrast, Bristol VP1 may be inefficiently or non-specifically encapsidated into SA11 VLPs. It is important to note that co-expression of Bristol VP2 and Bristol VP6 (irrespective of the presence or absence of Bristol VP1) results in the formation of aggregates that are morphologically inconsistent with VLPs (Table 1 and data not shown). Thus, at this time, we are not able to experimentally validate the capacity of Bristol VP1 to be encapsidated into cognate particles. It is possible that additional, as of yet unidentified, viral proteins may be required the formation of Bristol VLPs in the insect cell expression system.

SA11 VP2 NTD regions critical for efficient VP1 encapsidation

To determine which VP2 NTD regions are involved in efficient SA11 VP1 encapsidation into VLPs, we employed two different recombinant baculoviruses that express mutant SA11 core shell proteins missing either the first 10 NTD residues (Δ10 VP2), which are implicated in RNA-binding, or the entire NTD (Δ102 VP2), which is implicated in binding both RNA and the VP1/VP3 enzyme complex (Fig. 4). Sf9 cells were co-infected with baculoviruses expressing SA11 VP6 and either WT SA11 VP2 (WT VP2), Δ10 VP2 or Δ102 VP2 in the presence or absence of SA11 VP1- or Bristol VP1-expressing baculoviruses. VLPs were purified from the infected cell

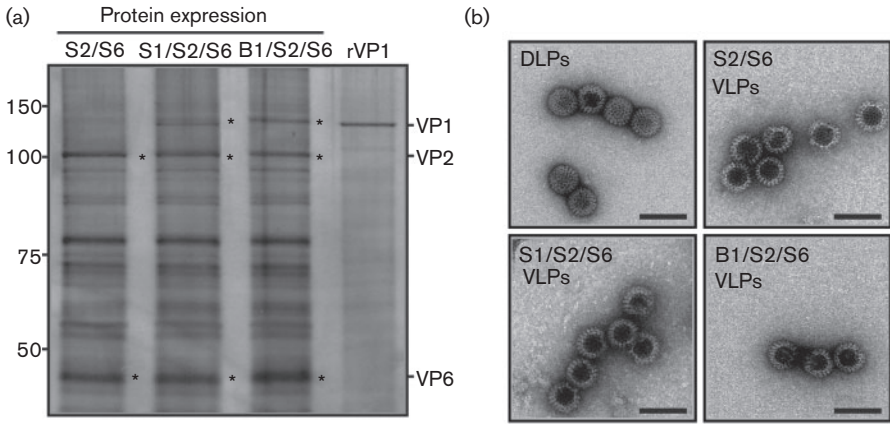

Fig. 2. Protein expression and VLP morphology. (a) Sf9 cells were infected with recombinant baculoviruses expressing SA11 VP2 and SA11 VP6 in the absence (S2/S6) or presence of SA11 VP1 (S1/S2/S6) or Bristol VP1 (B1/S2/S6). Infected Sf9 cells were lysed at 3 days p.i., and proteins were analysed by SDS-PAGE and silver staining. Molecular mass markers are shown in kilodaltons, and purified recombinant SA11 VP1 (rVP1) was run in the gel as an additional electrophoresis standard. (b) Native SA11 DLPs and VLPs (purified from the infected cell culture medium) were stained with 1 % uranyl acetate and visualized using EM. Bar, 100 nm.

supernatant at 5 days p.i. as described above, and particle formation was confirmed by negative-stain EM (Fig. 4a). No major ultrastructural differences were seen among VLPs made with WT VP2 versus the NTD mutant VP2 proteins, suggesting that the truncations did not prevent core formation, consistent with previous studies (Lawton *et al.*, 1997b; Zeng *et al.*, 1998) (Fig. 4a). We next assessed polymerase packaging by analysing the VLP protein composition using SDS-PAGE and silver staining (Fig. 4b). The results show that the VP2 and VP6 capsid proteins were detected in all samples, as expected (Fig. 4b). Surprisingly, SA11 VP1 was detected in the S1/S2/S6 VLPs made using Δ10 VP2, as well as those made using WT VP2 (Fig. 4b). In contrast, no obvious VP1 bands were detected in the S1/S2/S6 VLPs made using Δ102 VP2 or in any of the B1/S2/S6 VLPs (Fig. 4b). Quantification of protein levels in S1/S2/S6 VLPs made with Δ10 VP2 showed VP1:VP2 stoichiometry that approximated 1 : 10 (data not shown). These results suggest that NTD residues 1–10 are not essential for efficient polymerase packaging into VLPs, while NTD residues 11–102 are critical.

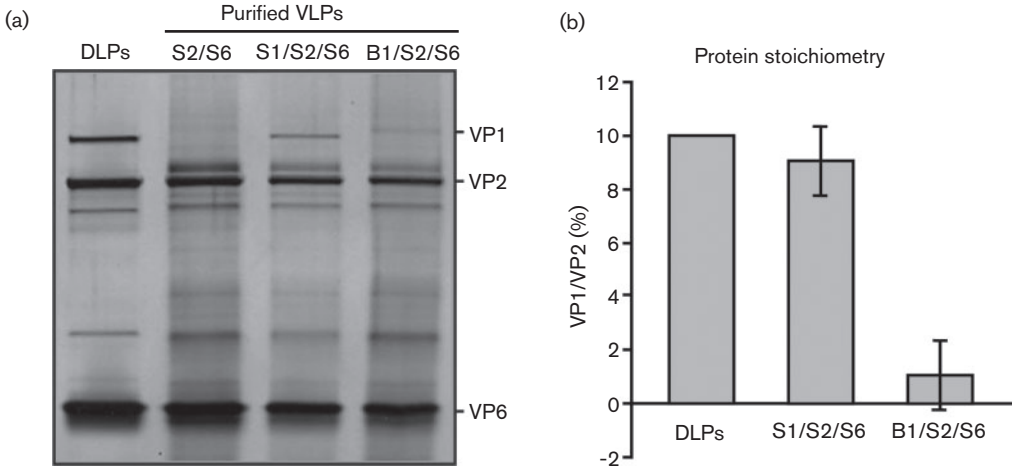

Fig. 3. Efficient encapsidation of SA11 VP1 into VLPs. (a) Protein components of purified VLPs were visualized following SDS-PAGE and silver staining. Native DLPs were used as molecular mass standards for the migration of VP1, VP2 and VP6. (b) Levels of VP1 and VP2 were quantified. The percentage of VP1 relative to VP2 for SA11 DLPs was normalized to 10.0. Results show the mean ± SD of four independent experiments.

Table 1. Summary of VP2 proteins assayed for VP1 encapsidation and activation

VP2	VP1	Encapsidation	Activation*
WT SA11	SA11	Yes	Yes (*robust*)
WT SA11	Bristol	No	No
Δ10 SA11	SA11	Yes	Yes (*minimal*)
Δ10 SA11	Bristol	No	No
Δ102 SA11	SA11	No	No
Δ102 SA11	Bristol	No	No
CHIM	SA11	Yes	Yes (*robust*)
CHIM	Bristol	No	No
Bristol	SA11	Unknown†	No
Bristol	Bristol	Unknown†	Yes (*robust*)

*Based on results of McDonald & Patton (2011b).
†Bristol VLPs did not form.

The observation that deletion of SA11 VP2 NTD residues 1–10 did not affect the capacity of the core shell protein to package the polymerase was unexpected, given that polymerase activation by this mutant was minimal (McDonald & Patton, 2011b) (Table 1). It is possible that the extreme amino terminus of VP2 plays an important role during genome replication that is distinct from VP1 interactions. This region of VP2 contains a high proportion of positively charged amino acids and is implicated in binding to viral RNA (Labbé *et al.*, 1994). Perhaps these first residues of VP2 engage viral RNA and aid in proper template presentation to the polymerase. Less surprising was the observation that deletion of the entire NTD (residues 1–102) resulted in no detectable VP1 encapsidation into VLPs. A similar result was shown using the core shell protein of bovine strain RF that lacks residues 1–92 (Zeng *et al.*, 1998). Δ102 VP2 was also not able to support any detectable VP1-mediated minus-strand RNA synthesis *in vitro*, demonstrating the importance of this inwardly protruding core shell region for effective polymerase interactions (McDonald & Patton, 2011b) (Table 1).

VP2 chimera that specifically activates SA11 VP1 also efficiently encapsidates SA11 VP1

To test whether the sequence of different VP2 regions is important for VP1 encapsidation, a recombinant baculovirus was employed that expresses an SA11 VP2 protein in which the NTD and dimer-forming subdomain was replaced with those of Bristol VP2 (Fig. 5a). Importantly, CHIM VP2 maintains the apical and carapace subdomains of SA11 VP2, which determine the strain specificity of VP1 during *in vitro* minus-strand RNA synthesis assays (McDonald & Patton, 2011b) (Table 1). Given the VP1 activation data, we hypothesized that VLPs made with

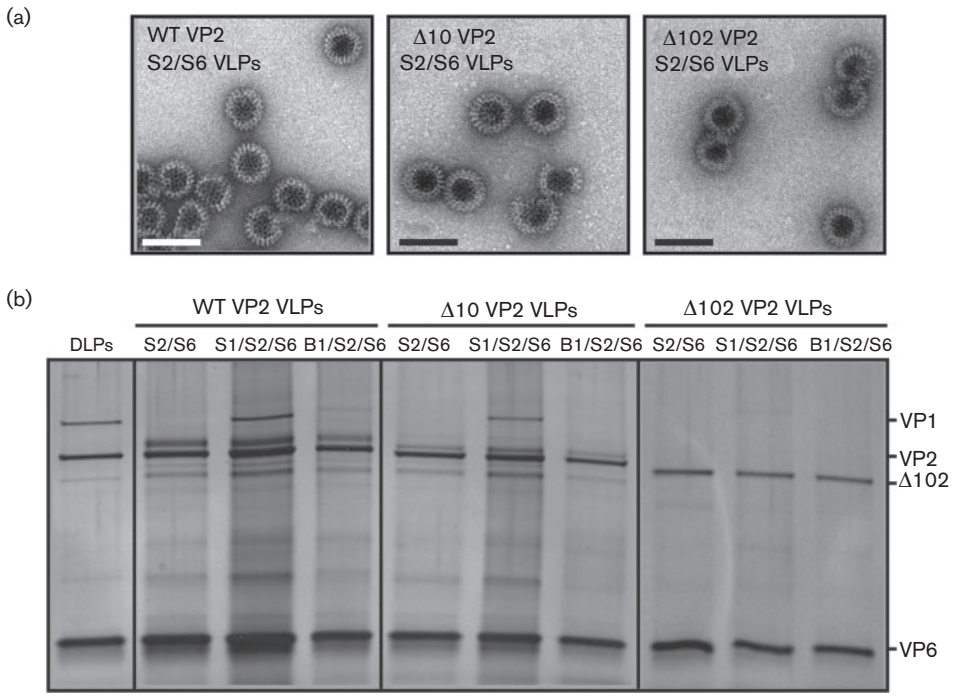

Fig. 4. VP1 packaging capacity of SA11 VP2 NTD truncation mutants. (a) VLPs purified from the infected cell culture medium were stained with 1 % uranyl acetate and imaged using EM. Bar, 100 nm. (b) Protein components of purified VLPs were visualized following SDS-PAGE and silver staining. Native SA11 DLPs were used as molecular mass standards for the migration of VP1, VP2 and VP6.

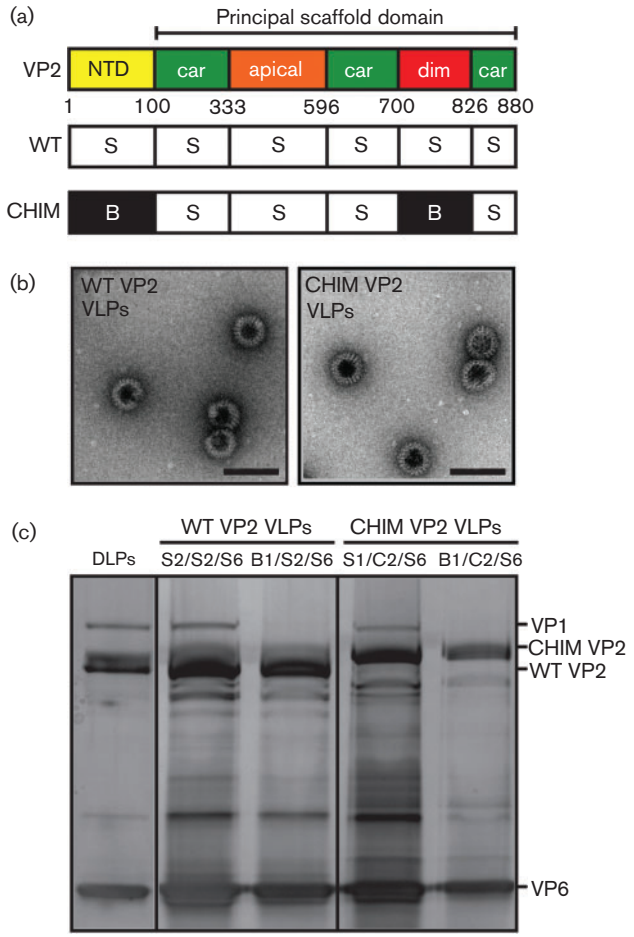

Fig. 5. VP1 packaging capacity of chimeric VP2. (a) In this cartoon schematic, the domains/subdomains of VP2 are coloured and labelled: NTD (yellow), apical subdomain (orange), carapace subdomain (green) and dimer-forming subdomain (red). The strain comprising each domain/subdomain of WT VP2 or the chimeric (CHIM) mutant VP2 is indicated: SA11 (S) or Bristol (B). (b) VLPs purified from the infected cell culture medium were stained with 1 % uranyl acetate and imaged using EM. Bar, 100 nm. (c) Protein components of purified VLPs were visualized following SDS-PAGE and silver staining. Native SA11 DLPs were used as molecular mass standards for the migration of VP1, VP2 and VP6. VLPs made by co-expression of CHIM VP2 and SA11 VP6, with either SA11 VP1 or Bristol VP1 are abbreviated S1/C2/S6 or B1/C2/S6, respectively.

CHIM VP2 would efficiently encapsidate SA11 VP1, but not Bristol VP1. To test this hypothesis, Sf9 cells were co-infected with baculoviruses expressing SA11 VP6, WT VP2 or CHIM VP2, and either SA11 VP1 or Bristol VP1. As before, VLPs were purified from the infected cell supernatant and particle formation was verified by negative-stain EM (Fig. 5b). We found no obvious differences in the particle morphology of CHIM VP2 VLPs versus WT VP2 VLPs, suggesting that the mutations did not grossly affect core formation (Fig. 5b). SDS-PAGE and silver staining of the VLP preparations revealed that SA11 VP1 was detected in S1/S2/S6 preparations generated with both WT VP2 and CHIM VP2 (Fig. 5c). In contrast, no obvious Bristol VP1 band was detected in either of the VLPs (Fig. 5c).

The observation that CHIM VP2 efficiently encapsidates SA11 VP1 indicates that the Bristol VP2 NTD and dimer-forming subdomain can functionally substitute for those regions of SA11 VP2. In fact, CHIM VP2 is indistinguishable from WT VP2 in its capacity to *both* package and activate SA11 VP1, indicating that the mutations do not disrupt polymerase binding (McDonald & Patton, 2011b) (Table 1). Given that SA11 VP2 and Bristol VP2 share minimal sequence conservation in their NTDs (<10 % amino acid identity), it is likely that this region of VP2 engages VP1 in a non-specific manner (Fig. 6a). Perhaps it is the structure or charged nature of the NTD (as opposed to the actual sequence) that is important for activation and packaging. Alternatively, the few residues that are conserved between SA11 VP2 and Bristol VP2 may be capable of maintaining the SA11 VP1 interaction. For example, Leu78 and Thr80 are shared between the divergent NTDs and comprise a structurally-resolved portion of VP2 that is seen extending into VP1 in the context of a DLP crystal (Estrozi *et al.*, 2012) (Fig. 6b). While the VP2 dimer-forming subdomain is also functionally interchangeable between strains SA11 and Bristol, this region of the core shell protein is unlikely to interact directly with VP1 given its peripheral location. Instead, we predict that there are, as of yet undefined, interactions between the VP2 NTD and dimer-forming subdomain that enhance the capacity of the NTD to bind VP1.

Based on the cumulative data, residues of the apical and/or carapace subdomains (rather than the NTD or dimer-forming subdomain) are hypothesized to be very important for the specificity of polymerase interactions. In the crystal structure of the DLP, VP1 is located just off-centre from the icosahedral fivefold axis with a binding footprint that overlaps the apical subdomains of neighbouring monomers (Estrozi *et al.*, 2012) (Fig. 6c). Internal portions of the apical subdomain seem to directly engage the polymerase in this static structure (Fig. 6b). Ongoing and future experiments in the lab are aimed at testing the hypothesis that these VP2 apical subdomains regions bind to the polymerase, resulting in its simultaneous packaging and activation. In this manner, the VP2 NTD would cradle VP1 from beneath, thereby keeping the enzyme anchored to the core shell and in a proper position for its enzymic activities during genome replication and transcription (Fig. 6c). Revealing the dynamic and multifaceted interactions between VP1 and VP2 during rotavirus core assembly is expected to contribute to our base knowledge of this paediatric pathogen and enhance rational antiviral and vaccine design.

METHODS

Cells and baculoviruses. Sf9 cells were grown in suspension flasks at 25 °C and maintained in complete Grace's insect cell medium

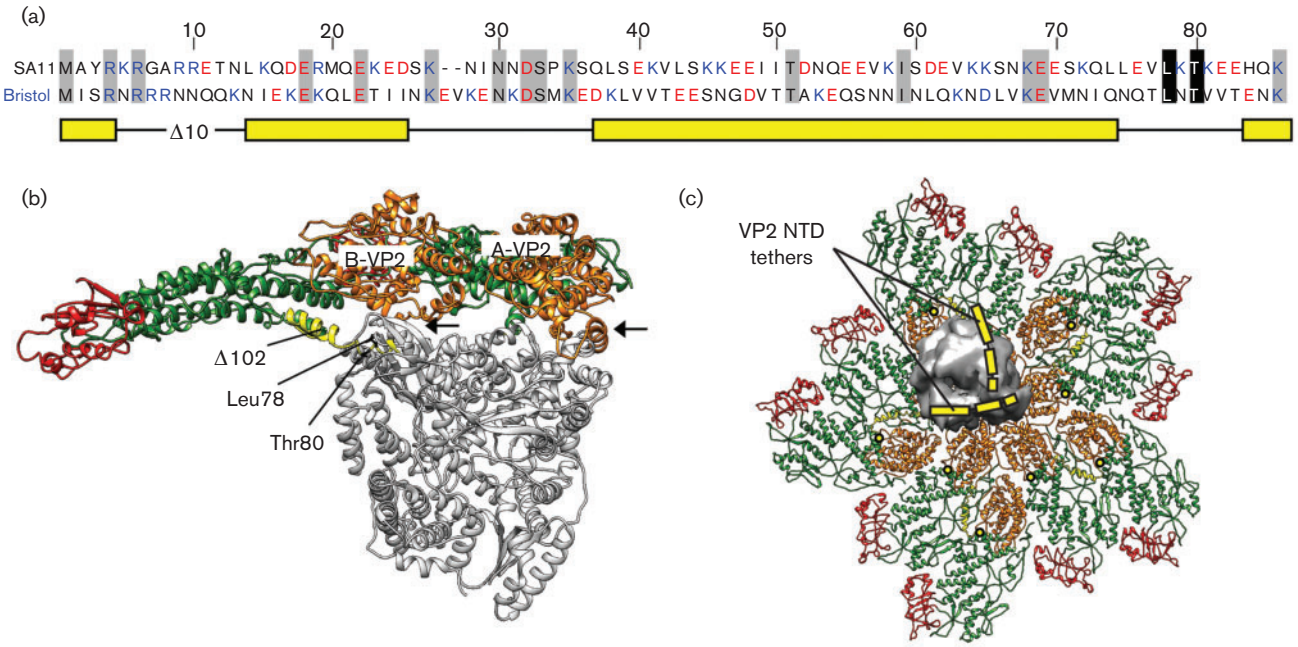

Fig. 6. VP2 residues that are probably involved in functional VP1 interactions. (a) The NTD amino acids of SA11 VP2 and Bristol VP2 are shown. Dashes indicate gaps in the protein sequence, and numbering corresponds to strain SA11. Positively and negatively charged residues are coloured blue and red, respectively. Regions of the NTD predicted to form α-helices are indicated by the yellow rectangles below the sequences. Grey shading highlights residues conserved between SA11 VP2 and Bristol VP2, but for which we do not have resolved structural locations. Two black shaded residues (Leu78 and Thr80) are conserved between SA11 VP2 and Bristol VP2 and are visualized in a known structure. The site of the Δ10 VP2 truncation is indicated. (b) Two neighbouring VP2 monomers (A-VP2 and B-VP2) of a decamer unit (side view; PDB#4F5X) are shown in ribbon representation and coloured according to Fig. 1. VP1 (grey) is also shown in ribbon representation bound to the inner surface of VP2. Residues Leu78 and Thr80 of the VP2 NTD are coloured black and labelled. Regions of the apical subdomain predicted to engage VP1 during core assembly and genome replication are indicated with arrows. The site of the Δ102 VP2 truncation is indicated. (c) Rendering of monomeric VP1 (grey; surface representation) bound to decameric VP2 (inside view). The VP2 decamer is shown in ribbon representation and rotated 90° backward compared with (b), so as to view the inside surface of the core shell. The VP2 NTD of each monomer is thought to the engage VP1 and possibly cradle the enzyme from beneath. For simplicity, two of these VP2 NTD tethers (not drawn to scale) are shown in cartoon form as connected yellow rectangles over the top of VP1. The location of residue 101 on each VP2 monomer is indicated with a yellow dot.

supplemented to contain 10 % heat-inactivated FBS (HyClone), 100 U penicillin ml^{-1} combined with 100 µg streptomycin ml^{-1} (Gibco), 0.5 µg Amphotericin B ml^{-1} (Fisher Scientific), and 1 % Pluronic F68 (Gibco). Recombinant baculoviruses expressing Bristol VP1, SA11 VP1, SA11 VP2 (WT VP2), Δ10 VP2, Δ102 VP2 and CHIM VP2 were generated as described previously (McDonald & Patton, 2011b). The SA11 VP6-expressing baculovirus was generated using the BaculoDirect C-Term kit (Life Technologies) according to the manufacturer's instructions. Briefly, the SA11-4F VP6-coding region was cloned into the pENTR-1A vector and subsequently transferred into the baculovirus genome using LR Clonase II. The baculovirus DNA was then transfected into Sf9 cells, and recombinant virus was selected for by growth in gancyclovir-containing medium.

Viral infection and protein expression. Sf9 cells grown in complete Grace's medium were pelleted for 1 min at 500 ***g*** at 25 °C and gently resuspended in serum-free Grace's medium at a density of 1×10^6 cells ml^{-1}. Cells were infected with the indicated baculoviruses at an m.o.i. ⩾5 and incubated in suspension flasks at 28 °C. Protease inhibitors, leupeptin and aprotinin, were added to the cultures daily at a final concentration of 1 µg ml^{-1}. At 3 days p.i., 1 ml aliquots of cells were taken to verify recombinant protein expression. Infected cells were washed twice with cold PBS, resuspended in 10 ml of cold lysis buffer (25 mM $NaHPO_4$, 200 mM NaCl, pH 7.8), and sonicated. The insoluble fraction was removed by centrifugation at 15 000 ***g*** for 10 min at 4 °C. Approximately 20 µl of cleared lysates were electrophoresed in a 7.5 % SDS-polyacrylamide gel and processed with the SilverQuest silver staining kit (Life Technologies) according to the manufacturer's instructions. The Precision Plus Protein Kaleidoscope Standard (Bio-Rad) was used as a molecular mass marker. Purified rVP1 was generated as described previously and also used as an electrophoresis standard (McDonald & Patton, 2011b).

Purification of VLPs and analysis of protein composition. The cell culture medium from infected Sf9 cells was collected at 5 days p.i. and clarified by centrifugation for 5 min at 1500 ***g*** and 4 °C. Large protein complexes (including VLPs) that were released into the medium during infection were first concentrated by pelleting through a 35 % (w/v) sucrose cushion in TNE buffer (20 mM Tris, pH 7.4, 50 mM NaCl, 1 mM EDTA) for 1.5 h at 80 000 ***g*** and 4 °C. The

protein pellet was resuspended in TNE containing complete protease inhibitor tablets (Roche), and VLPs were further purified by isopycnic centrifugation in caesium chloride (density 1.28–1.31 g cm^{-3}) for 16 h at 110 000 ***g*** and 12 °C. Visible protein bands were collected in 500 µl fractions from each gradient and dialysed exhaustively against TNE buffer. All purified VLP preparations were stored at 4 °C in the presence of 1 µg ml^{-1} aprotinin and leupeptin. In general, ~10 µg of VLPs (total protein) was generated from 5×10^7 infected Sf9 cells.

Approximately 400 ng of each purified VLP preparation was electrophoresed in 7.5 % SDS-polyacrylamide gels and stained using the SilverQuest kit. The Precision Plus Protein Kaleidoscope Standard (Bio-Rad) was used as a molecular mass marker. Native SA11 DLPs were generated as described previously and were also used as an electrophoresis standard (Bican *et al.*, 1982). VP1 and VP2 protein levels in stained gels were quantified using a ChemiDoc Gel Imaging System (Bio-Rad). The percentage of VP1 relative to VP2 in DLP preparations were normalized to 10.0.

Negative-stain specimen preparation and electron microscopy. Copper EM grids (400 mesh; Ted Pella) containing continuous carbon support films were glow discharged for 1 min using a Pelco EasiGlow System (Ted Pella). Aliquots of VLPs (3 µl each) were absorbed to the EM grids for 1 min and negatively stained for 15 s using 1 % uranyl acetate (pH 7.5). Specimens were examined using an FEI Spirit BioTwin Transmission EM (FEI Company) equipped with a LaB_6 filament operating at 120 kV. Images were recorded on a FEI Eagle 2k HS CCD camera, and the sampling in the images is 10 Å per pixel at the specimen level.

Amino acid alignment and structure analysis. The VP2 NTD amino acid alignment was constructed with Geneious Pro v5.5.2 using the CLUSTAL W plugin with the BLOSUM cost matrix. Secondary structure predictions of the VP2 NTD were implemented via Geneious Pro v5.5.2 using the Garnier Osguthorpe Robson algorithm provided by the EMBOSS suite (Rice *et al.*, 2000). Three dimensional structure analysis of VP2 (PDB#3KZ4) and VP1-VP2 (PDB#4F5X) was performed using UCSF Chimera-Molecular Molecular Modelling System (Estrozi *et al.*, 2012; Pettersen *et al.*, 2004; McClain *et al.*, 2010).

ACKNOWLEDGEMENTS

The authors would like to thank John T. Patton (National Institutes of Health) for providing the published reagents used in these studies. We also thank Paul McDonald and Allison McKell for editorial suggestions on the manuscript. This work was financed by new investigator start-up funds from the Virginia Tech Carilion Research Institute.

REFERENCES

Bican, P., Cohen, J., Charpilienne, A. & Scherrer, R. (1982). Purification and characterization of bovine rotavirus cores. *J Virol* **43**, 1113–1117.

Crawford, S. E., Labbé, M., Cohen, J., Burroughs, M. H., Zhou, Y. J. & Estes, M. K. (1994). Characterization of virus-like particles produced by the expression of rotavirus capsid proteins in insect cells. *J Virol* **68**, 5945–5952.

Estes, M. K. & Kapikian, A. Z. (2007). Rotaviruses. In *Fields Virology*, 2nd edn, vol. 2, pp. 1917–1974. Edited by D. M. Knipe & D. M. Howley. Philadelphia: Lippincott Williams and Wilkins.

Estrozi, L. F., Settembre, E. C., Goret, G., McClain, B., Zhang, X., Chen, J. Z., Grigorieff, N. & Harrison, S. C. (2013). Location of the dsRNA-dependent polymerase, VP1, in rotavirus particles. *J Mol Biol* **425**, 124–132.

Guglielmi, K. M., McDonald, S. M. & Patton, J. T. (2010). Mechanism of intraparticle synthesis of the rotavirus double-stranded RNA genome. *J Biol Chem* **285**, 18123–18128.

Jayaram, H., Estes, M. K. & Prasad, B. V. (2004). Emerging themes in rotavirus cell entry, genome organization, transcription and replication. *Virus Res* **101**, 67–81.

Labbé, M., Baudoux, P., Charpilienne, A., Poncet, D. & Cohen, J. (1994). Identification of the nucleic acid binding domain of the rotavirus VP2 protein. *J Gen Virol* **75**, 3423–3430.

Lawton, J. A., Estes, M. K. & Prasad, B. V. (1997a). Three-dimensional visualization of mRNA release from actively transcribing rotavirus particles. *Nat Struct Biol* **4**, 118–121.

Lawton, J. A., Zeng, C. Q., Mukherjee, S. K., Cohen, J., Estes, M. K. & Prasad, B. V. (1997b). Three-dimensional structural analysis of recombinant rotavirus-like particles with intact and amino-terminal-deleted VP2: implications for the architecture of the VP2 capsid layer. *J Virol* **71**, 7353–7360.

Li, Z., Baker, M. L., Jiang, W., Estes, M. K. & Prasad, B. V. (2009). Rotavirus architecture at subnanometer resolution. *J Virol* **83**, 1754–1766.

McClain, B., Settembre, E., Temple, B. R., Bellamy, A. R. & Harrison, S. C. (2010). X-ray crystal structure of the rotavirus inner capsid particle at 3.8 A resolution. *J Mol Biol* **397**, 587–599.

McDonald, S. M. & Patton, J. T. (2011a). Assortment and packaging of the segmented rotavirus genome. *Trends Microbiol* **19**, 136–144.

McDonald, S. M. & Patton, J. T. (2011b). Rotavirus VP2 core shell regions critical for viral polymerase activation. *J Virol* **85**, 3095–3105.

McDonald, S. M., Aguayo, D., Gonzalez-Nilo, F. D. & Patton, J. T. (2009). Shared and group-specific features of the rotavirus RNA polymerase reveal potential determinants of gene reassortment restriction. *J Virol* **83**, 6135–6148.

Parashar, U. D., Burton, A., Lanata, C., Boschi-Pinto, C., Shibuya, K., Steele, D., Birmingham, M. & Glass, R. I. (2009). Global mortality associated with rotavirus disease among children in 2004. *J Infect Dis* **200** (Suppl 1), S9–S15.

Patton, J. T. & Spencer, E. (2000). Genome replication and packaging of segmented double-stranded RNA viruses. *Virology* **277**, 217–225.

Patton, J. T., Jones, M. T., Kalbach, A. N., He, Y. W. & Xiaobo, J. (1997). Rotavirus RNA polymerase requires the core shell protein to synthesize the double-stranded RNA genome. *J Virol* **71**, 9618–9626.

Pesavento, J. B., Crawford, S. E., Estes, M. K. & Prasad, B. V. (2006). Rotavirus proteins: structure and assembly. *Curr Top Microbiol Immunol* **309**, 189–219.

Pettersen, E. F., Goddard, T. D., Huang, C. C., Couch, G. S., Greenblatt, D. M., Meng, E. C. & Ferrin, T. E. (2004). UCSF Chimera–a visualization system for exploratory research and analysis. *J Comput Chem* **25**, 1605–1612.

Prasad, B. V., Rothnagel, R., Zeng, C. Q., Jakana, J., Lawton, J. A., Chiu, W. & Estes, M. K. (1996). Visualization of ordered genomic RNA and localization of transcriptional complexes in rotavirus. *Nature* **382**, 471–473.

Rice, P., Longden, I. & Bleasby, A. (2000). EMBOSS: the European Molecular Biology Open Software Suite. *Trends Genet* **16**, 276–277.

Settembre, E. C., Chen, J. Z., Dormitzer, P. R., Grigorieff, N. & Harrison, S. C. (2011). Atomic model of an infectious rotavirus particle. *EMBO J* **30**, 408–416.

Tortorici, M. A., Broering, T. J., Nibert, M. L. & Patton, J. T. (2003). Template recognition and formation of initiation complexes by the replicase of a segmented double-stranded RNA virus. *J Biol Chem* **278**, 32673–32682.

Zeng, C. Q., Wentz, M. J., Cohen, J., Estes, M. K. & Ramig, R. F. (1996). Characterization and replicase activity of double-layered and single-layered rotavirus-like particles expressed from baculovirus recombinants. *J Virol* **70**, 2736–2742.

Zeng, C. Q., Estes, M. K., Charpilienne, A. & Cohen, J. (1998). The N terminus of rotavirus VP2 is necessary for encapsidation of VP1 and VP3. *J Virol* **72**, 201–208.

Zhang, X., Settembre, E., Xu, C., Dormitzer, P. R., Bellamy, R., Harrison, S. C. & Grigorieff, N. (2008). Near-atomic resolution using electron cryomicroscopy and single-particle reconstruction. *Proc Natl Acad Sci U S A* **105**, 1867–1872.